

## Chiral Phonons at High-Symmetry Points in Monolayer Hexagonal Lattices

Lifa Zhang<sup>1,2</sup> and Qian Niu<sup>1,3</sup>

<sup>1</sup>*Department of Physics, The University of Texas at Austin, Austin, Texas 78712, USA*

<sup>2</sup>*Department of Physics and Institute of Theoretical Physics, Nanjing Normal University, Nanjing 210023, China*

<sup>3</sup>*International Center for Quantum Materials, Peking University, Beijing 100871, China*

(Received 9 February 2015; published 11 September 2015)

In monolayer hexagonal lattices, the intravalley and intervalley scattering of electrons can involve chiral phonons at Brillouin-zone center and corners, respectively. At these high-symmetry points, there is a threefold rotational symmetry endowing phonon eigenmodes with a quantized pseudoangular momentum, which includes orbital and spin parts. Conservation of pseudoangular momentum yields selection rules for intravalley and intervalley scattering of electrons by phonons. Concrete predictions of helicity-resolved optical phenomena are made on monolayer molybdenum disulfide. The chiral phonons at Brillouin-zone corners excited by polarized photons can be detected by a valley phonon Hall effect. The chiral phonons, together with phonon circular polarization, phonon pseudoangular momentum, selection rules, and valley phonon Hall effect will extend the basis for valley-based electronics and phononics applications in the future.

DOI: 10.1103/PhysRevLett.115.115502

PACS numbers: 63.22.-m, 72.10.Di

Because of inversion symmetry breaking, valley-contrasting electronic physics proposed by Xiao *et al.* in 2007 [1] has attracted a growing interest in the manipulation of the valley degree of electrons since it has potential applications in valley-dependent optoelectronics [2] and coupled spin and valley physics [3]. Besides charge and spin, separated valleys in momentum space constitute another discrete degree of freedom for electrons with a long relaxation time, which leads to the emergence of valleytronics, such as valley polarization, valley current, and valley coherence on transition-metal dichalcogenide (TMD) materials [4–10]. The valley electron interband scattering involves a polarized photoexcitation and photoluminescence; however, the intervalley electron scattering will involve Brillouin-zone-corner (valley) phonons [7]. Given the fact that electrons have definite chirality at valleys, two natural questions then arise: do valley phonons have chirality and what role does the chirality play in electronic intervalley scattering?

Very recently, the helicity-resolved Raman scattering has been experimentally observed in TMD atomic layers [11], where the authors found that Brillouin-zone-center ( $\Gamma$ ) phonons can completely reverse the helicity of incident photons. Such a finding implies that besides the valley phonons, the  $\Gamma$  phonons involved in the intravalley scattering of electrons can also have chirality. Therefore, it is highly desirable to investigate phonon chirality at these high-symmetry points in the Brillouin zone of the hexagonal lattices and also their applications in valleytronics.

In this Letter, we observe chiral phonons at the Brillouin-zone center and the corners of the honeycomb lattices. The threefold rotational symmetry at these high-symmetry points allows us to label phonon eigenmodes with

pseudoangular momentum (PAM). The lack of inversion symmetry within the plane and the fact that time reversal symmetry is broken at the  $K$  and  $K'$  points are the fundamental reasons why valley phonon modes are non-degenerate and have definite PAM. At the  $\Gamma$  point where time reversal symmetry is presented, phonon modes with opposite pseudoangular momenta become degenerate. The chirality of phonons at these high-symmetry points not only decides the selection rules in both intravalley and intervalley electronic scattering but also can endow phononics with other potential effects, e.g., valley phonon Berry curvature and the valley phonon Hall effect. And near these high-symmetry points a phonon has extremes in dispersion and thus a large density of states. Therefore, chiral phonons will play an important role in valleytronics, especially in the intravalley or intervalley scattering of electrons or holes.

*Chirality of phonons.*—To study chiral phonons, we first focus on a two-dimensional honeycomb lattice model, where each unit cell has two sublattices,  $A$  and  $B$ . The honeycomb  $AB$  lattice can serve as a simplified model to demonstrate general features of chiral phonons in monolayer materials, such as gapped graphene with isotopic doping [12] or staggered sublattice potential [13], hexagonal boron nitride [14]. From calculated eigenvectors, we can plot sublattice vibrations at valleys as shown in the insets of Fig. 1(a). At valleys, all of the vibrations are circularly polarized. For valley phonon modes of bands 1 and 4, the two sublattices make opposite circular motions; for bands 2 and 3 while one sublattice is still, the other sublattice makes a circular motion. From valley  $K$  to  $K'$ , all of the circular motions will change to the opposite direction; thus, in later discussions we will focus on one

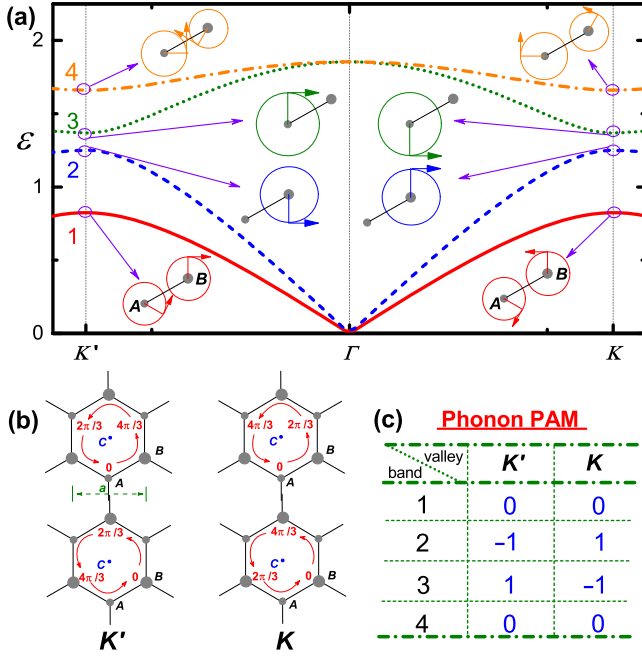


FIG. 1 (color online). Valley phonons in a honeycomb  $AB$  lattice. (a) Phonon dispersion relation of a honeycomb  $AB$  lattice. The insets show phonon vibrations for sublattices  $A$  and  $B$  in one unit cell at  $K'$  ( $k_x = -(4\pi/3a)$ ,  $k_y = 0$ ) and  $K$  ( $k_x = (4\pi/3a)$ ,  $k_y = 0$ ), numbers 1 to 4 denote four bands. The radii of circles denote vibration amplitudes; phase and rotation direction are included. (b) Phase correlation of the phonon nonlocal part for sublattice  $A$  (upper two panels) and sublattice  $B$  (lower two panels) at  $K'$  (left panels) and  $K$  (right panels). (c) Phonon pseudoangular momentum (PAM) for bands 1 to 4 at valleys  $K'$  and  $K$ . Here, the longitudinal spring constant  $K_L = 1$ , the transverse one  $K_T = 0.25$ , and  $m_A = 1$ ,  $m_B = 1.2$ . The primitive vectors are  $(a, 0)$  and  $(a/2, \sqrt{3}a/2)$ , and the phonon energy  $\epsilon$  is equal to  $\hbar\omega_{\text{ph}}$ .

of the valleys, while results at the other one are achieved by time reversal symmetry.

The phonon chirality can be characterized by the polarization of phonons, which comes from the circular vibration of sublattices. To consider the polarization along the  $z$  direction, we look at the phonon eigenvectors  $\epsilon = (x_1, y_1, x_2, y_2)^T$  (here we take a two-sublattice unit cell as an example; for a general case, see the Supplemental Material, Sec. I [15]). By defining a new basis where one sublattice has right-handed or left-handed circular polarization as  $|R_1\rangle \equiv \frac{1}{\sqrt{2}}(1 \ i \ 0 \ 0)^T$ ,  $|L_1\rangle \equiv \frac{1}{\sqrt{2}}(1 \ -i \ 0 \ 0)^T$ ,  $|R_2\rangle \equiv \frac{1}{\sqrt{2}}(0 \ 0 \ 1 \ i)^T$ , and  $|L_2\rangle \equiv \frac{1}{\sqrt{2}}(0 \ 0 \ 1 \ -i)^T$ , the phonon eigenvector  $\epsilon$  can be represented as

$$\epsilon = \sum_{\alpha=1}^n \epsilon_{R_\alpha} |R_\alpha\rangle + \epsilon_{L_\alpha} |L_\alpha\rangle, \quad (1)$$

where  $\epsilon_{R_\alpha} = \langle R_\alpha | \epsilon \rangle = \frac{1}{\sqrt{2}}(x_\alpha - iy_\alpha)$ ,  $\epsilon_{L_\alpha} = \langle L_\alpha | \epsilon \rangle = \frac{1}{\sqrt{2}}(x_\alpha + iy_\alpha)$ . Then, the operator for phonon circular polarization along the  $z$  direction can be defined as

$$\hat{S}^z \equiv \sum_{\alpha=1}^n (|R_\alpha\rangle\langle R_\alpha| - |L_\alpha\rangle\langle L_\alpha|), \quad (2)$$

and the phonon circular polarization is equal to

$$s_{\text{ph}}^z = \epsilon^\dagger \hat{S}^z \epsilon \hbar = \sum_{\alpha=1}^n (|\epsilon_{R_\alpha}|^2 - |\epsilon_{L_\alpha}|^2) \hbar, \quad (3)$$

here  $n = 2$  for two-sublattice unit cells. The phonon circular polarization can have a value between  $\pm\hbar$  since  $\sum_{\alpha} |\epsilon_{R_\alpha}|^2 + |\epsilon_{L_\alpha}|^2 = 1$ . The  $s_{\text{ph}}^z$  has the same form with that of phonon angular momentum  $j_{k,\sigma}^z$  along the  $z$  direction [19] (see the Supplemental Material, Sec. I [15]). The contribution from each sublattice in one unit cell to the phonon circular polarization is  $s_{\alpha}^z$ , which is equal to  $\epsilon^\dagger \hat{S}_{\alpha}^z \epsilon \hbar$ , with  $\hat{S}_{\alpha}^z = |R_\alpha\rangle\langle R_\alpha| - |L_\alpha\rangle\langle L_\alpha|$ . In Fig. 1(a), at valley  $K$ ,  $s_A^z = 0$ ,  $s_B^z = -\hbar$  for band 2, while  $s_A^z = \hbar$ ,  $s_B^z = 0$  for band 3, where the phonon circular polarization happens to be quantized; for bands 1 and 4, sublattices  $A$  and  $B$  create opposite circular vibrations with different magnitudes of  $s_{A,B}$ . Therefore, phonon circular polarization  $s_{\text{ph}}^z$  at the valleys can be nonzero. By introducing a staggered sublattice on-site potential, the similar chiral phonons at valleys can also be observed, and the chiral valley phonons can be observed in graphene systems with introducing isotope doping (see the Supplemental Material, Secs. II and III [15]).

At the zone center  $\Gamma$ , as shown in Fig. 1(a), there are doubly degenerate acoustic modes and doubly degenerate optical modes which are not circularly polarized; however, we can obtain circular polarized phonon modes by superposition of the degenerated modes.

*Phonon pseudoangular momentum.*—In a honeycomb lattice, at high-symmetry points  $\Gamma, K, K'$ , phonons are invariant under a threefold discrete rotation about the direction ( $z$ ) perpendicular to the lattice plane. Under the rotation, one can obtain  $\mathfrak{R}[(2\pi/3), z] u_{\mathbf{k}} = e^{-i(2\pi/3)l_{\text{ph}}^{\mathbf{k}}} u_{\mathbf{k}}$ , where  $l_{\text{ph}}^{\mathbf{k}}$  is defined as the PAM of a phonon with wave function  $u_{\mathbf{k}}$  and has values of  $\pm 1$  or  $0$ . The phase correlation of the phonon wave function comes from two parts: one is from the local (intracell) part  $\epsilon_{k,\sigma}$ , another is from the nonlocal (intercell) part  $e^{i\mathbf{R} \cdot \mathbf{k}}$ . Thus, under a threefold rotation, one can obtain spin PAM  $l^s$  for the local part and orbital PAM  $l^o$  for the nonlocal part.

The orbital PAM can be obtained from a phase change under a threefold rotation, which is shown in Fig. 1(b). We can obtain  $l_A^o = \tau$  and  $l_B^o = -\tau$ ,  $\tau = \pm 1$  labels the two valleys  $K$  and  $K'$ . At  $\Gamma$  point, there is no phase change for both sublattices under a threefold rotation; thus,  $l_A^o = l_B^o = 0$ . Both circular polarization  $|R_\alpha\rangle$  and  $|L_\alpha\rangle$  are eigenstates of the operator  $\mathfrak{R}[(2\pi/3), z]$ , with PAM  $l_R^s = 1$  and  $l_L^s = -1$ , respectively. Therefore, in Fig. 1(a), at valley  $K$ ,  $l_A^s = -1$ ,  $l_B^s = 1$  for bands 1 and 4,  $l_B^s = -1$  for band 2, and  $l_A^s = 1$  for band 3. Since phonon wave function must be an eigenstate of the rotation operator, the PAM of the

phonon equals  $l_{\text{ph}} = l_A^s + l_A^o = l_B^s + l_B^o$  if both sublattices are vibrating; if one is still, it is decided by the other vibrating sublattice. Therefore, we can obtain the phonon PAM as listed in Fig. 1(c). At  $\Gamma$  point,  $l_{\text{ph}} = l_A^s = l_B^s$  since the orbital PAM is zero. By superposition of the doubly degenerated modes, sublattices do the same circular vibration, which can be right handed or left handed. Thus, the phonon PAM can be  $\pm 1$  for doubly degenerated modes.

At high-symmetry points where the threefold rotational symmetry holds, the PAM of nondegenerate phonon modes must be  $\pm 1$  or zero. Since a threefold rotation center can be chosen at any sublattice in a unit cell when the orbital PAM of this sublattice will be zero, the spin PAM of the sublattice must be equal to the phonon PAM; that is, it must also be  $\pm 1$  or zero. Therefore, as shown in Fig. 1(a), for all phonon modes at valleys, sublattices must create circularly polarized vibrations; otherwise, they are still. For three-dimensional vibrations, the out-of-plane modes are also an eigenstate of the threefold rotation with a PAM of  $l_{\text{ph}} = 0$ .

**Selection rules.**—For electrons with a zero moment along the normal direction of the plane ( $z$ ), the state is invariant under a threefold rotation, the PAM is decided by the orbits on sublattice  $A$  or  $B$ . Based on the lattice structure in Fig. 1(b), if we assume that the valence band corresponds to the orbit on sublattice  $A$  and the conduction band corresponds to the orbit on sublattice  $B$ , we can obtain all the pseudoangular momenta  $l_{c(v)} = \mp\tau$ . Therefore, due to conservation of the PAM, one can expect an azimuthal selection rule  $l_c - l_v = l_{\text{photon}} = \pm\tau$  for the interband transition by photons with right ( $\sigma+$ ) or left ( $\sigma-$ ) circular polarization in the gapped graphene. The excited electron in the conduction band can have an intravalley scattering by a phonon at  $\Gamma$ , and it then combines with the hole in the valence band by emitting another photon. This process is called first order Raman scattering (e.g., the  $G$  peak in graphene). In this process, because of the conservation of the PAM, we have a selection rule  $\Delta l_{\text{photon}} = l_{\text{ph}}$ . The doubly degenerate optical modes at  $\Gamma$  are Raman active and have a pseudoangular momenta of  $\pm 1$ ; thus, we can expect a helicity-resolved Raman  $G$  peak in honeycomb lattices, which can be gapped graphene or a boron nitride monolayer. In the whole process, the incident right-(left-) handed photon absorbs a right-(left-) handed phonon or emits a left-(right-) handed phonon then changes its helicity to be a left- (right-) handed photon. Such a selection rule explains the helicity-resolved Raman scattering in layered TMD, as reported in Ref. [11]. For the out-of-plane phonon involving only chalcogen atoms as well as the low-energy breathing modes, they have  $l_{\text{ph}} = 0$ ; thus, the helicity of the incident photon will not change.

It is well known that in graphene the double resonance  $D$  peak in Raman spectrum is related to phonon modes in the vicinity of the  $K$  point during the intervalley scattering [20,21]. In the intervalley scattering by phonon the whole system has threefold rotational symmetry; thus, we can

expect a selection rule from the conservation of the PAM. That is,  $l_{c(v)}(\mathbf{K}) - l_{c(v)}(\mathbf{K}') = \pm 1$  by emitting a circularly polarized valley phonon ( $l_{\text{ph}} = \pm 1$ ), where momentum and energy conservations are also applied. Thus, we can expect that a valley phonon with a specific PAM can be created. Because the PAMs of valley phonons are different, we can observe a circularly polarized infrared spectrum during the valley phonon interband scattering (please see the Supplemental Material, Sec. IV for a detailed discussion [15]).

With spin-orbit coupling  $\text{MoS}_2$  has a band gap of  $\Delta = 1.65$  eV and a spin splitting for the highest valence band at  $\mathbf{K}$  valley  $\lambda_{Kv} = 150$  meV, as shown in Fig. 2, while for the lowest conduction band there is a 3 meV splitting, which may be negligible [22]. With a photon absorption or emission, we can expect to observe intervalley electron scattering at valley centers involving a valley center phonon, where the selection rules imply  $\Delta l_{\text{el}} = \pm l_{\text{ph}} \pm l_{\text{photon}}$  and  $\lambda_K = \pm \hbar\omega_{\text{ph}} \pm \hbar\omega_{\text{photon}}$ , where  $+$  means emission and  $-$  means absorption. For monolayer  $\text{MoS}_2$ , at valleys the PAM of electrons in the conduction band are  $\pm 1$ , while they are zero for the valence band [4]. Through a right-handed polarized photon a pair of exciton are excited at  $\mathbf{K}$  valley as shown in Fig. 2, where the blue lines correspond to the absorption of a right-handed photon with energy  $\Delta$ . Since the excited electron is in the valley center, which cannot be scattered to another valley through emitting a phonon. However, because of the large spin splitting of the valence band, the hole can be scattered to another valley by absorbing a stimulated circularly polarized photon and emitting a chiral valley phonon, where the spin of electron is fixed. Using the Quantum-Espresso code [23], we obtain phonons for all bands at valleys as shown in

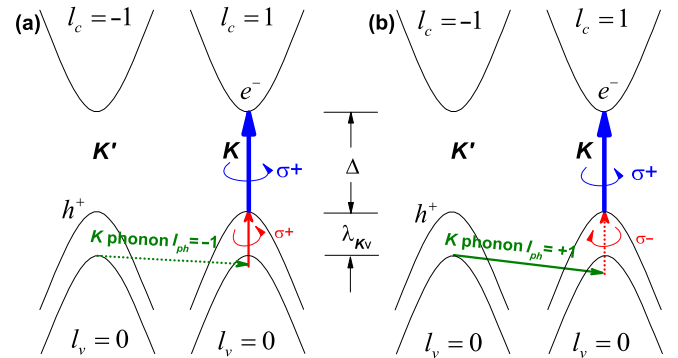


FIG. 2 (color online). Valley phonons emitted in hole intervalley scattering in  $\text{MoS}_2$ . The exciton is excited by a right polarized photon with energy ( $\Delta$ ) at  $\mathbf{K}$  valley. (a) By absorbing a stimulated right-handed photon with energy ( $\lambda_{Kv} + \hbar\omega$ ), the excited hole in the valence band is scattered to the other valley  $\mathbf{K}'$  by emitting a valley phonon with energy  $\hbar\omega$  and PAM  $l_{\text{ph}} = -1$ . (b) A stimulated left-handed photon is absorbed and a phonon with  $l_{\text{ph}} = 1$  is emitted. The pseudoangular momenta of electrons in the conduction band and the valence band [ $l_{v(c)} = \pm 1, 0$ ] are also marked.

TABLE I. Chiral phonons in the  $\mathbf{K}$  valley of  $\text{MoS}_2$ . Monolayer  $\text{MoS}_2$  has nine modes ( $n$ ) of phonon with energy  $\hbar\omega_{\text{ph}}$  (meV), Mo and S are located in  $A$  and  $B$ , respectively, as shown in Fig. 1(b) in the main text. Thus, the orbital PAM  $l_{\text{Mo}}^o = 1$  and  $l_{\text{S}}^o = -1$ .  $s_{\text{Mo}}^z$  ( $s_{\text{S}}^z$ ),  $l_{\text{Mo}}^s$  ( $l_{\text{S}}^s$ ), and  $l_{\text{ph}}$  are circular polarizations of Mo (S), spin pseudoangular momenta of Mo (S), and phonon PAM. The mirror symmetry ( $M_S$ ) is relative to the plane of the monolayer of  $\text{MoS}_2$ ; it is 1 (−1) if the mode is even (odd) under the mirror symmetry operation.

$n$	$\hbar\omega_{\text{ph}}$	$s_{\text{Mo}}^z$	$s_{\text{S}}^z$	$l_{\text{Mo}}^s$	$l_{\text{S}}^s$	$l_{\text{ph}}$	$M_S$
1	14.4	0.64	0	1	0	−1	1
2	21.5	0	−0.34	0	−1	1	−1
3	31.9	−0.18	0.41	−1	1	0	1
4	40.0	0	−0.50	0	−1	1	1
5	40.2	0	0	...	...	0	−1
6	41.5	0	0.50	0	1	0	1
7	45.1	0	−0.40	0	−1	1	−1
8	48.0	0.06	0	1	0	−1	1
9	49.2	−0.34	0.33	−1	1	0	1

Table I (see Supplemental Material, Sec. V [15]). At  $\mathbf{K}$  valley, phonons with energy 14.4 and 48.0 meV have a PAM of  $l_{\text{ph}} = -1$  and phonons of 21.5, 40.0, and 45.1 meV have an  $l_{\text{ph}}$  of 1.

As shown in Fig. 2(a), through a stimulated right-handed light scanning on the sample, we can observe a certain resonance peak on  $\lambda_{\mathbf{K}v} + \hbar\omega_{\text{ph}}$ , where the emitted chiral phonon carries a PAM of  $l_{\text{ph}} = -1$  at the  $\mathbf{K}$  point due to the selection rules at the valleys. The resonance peak is at 164.4 meV (another peak of 198.0 meV is not obvious due to the small polarization of the 48.0 meV phonon). And for a stimulated left-handed photon in Fig. 2(b), we can only observe one peak of 190.0 meV corresponding to a phonon mode of 40.0 meV, while the other two modes will not be involved because they are odd under the mirror operation (see Table I) since in the scattering process the whole system keeps even under a mirror operation relative to the  $x - y$  plane. After being scattered by phonon and photon, the electron and hole pair locates in different valleys, which is consistent with the recent finding of low-energy excitons with a large momentum [24]. Similarly, a chiral phonon at  $\mathbf{K}'$  can be emitted in the scattering of the hole of an exciton at a  $\mathbf{K}'$  valley which can be excited by a left-handed photon with 1.65 eV. Therefore, a specific chiral phonon at a definite valley can be obtained through a stimulated photon. With the two-step polarized light shining on the sample, a large number of valley phonons with definite frequencies can be created.

*Valley phonon Hall effect.*—In the presence of an in-plane electric field, an electron will acquire an anomalous velocity proportional to the Berry curvature in the transverse direction [25,26]. Recently, the electronic valley Hall effect proposed in Ref. [1] has been experimentally observed in monolayer  $\text{MoS}_2$  transistors [27] and in graphene superlattices [28]. As was discussed above, phonons with definite frequencies at a specific valley can be massively created; thus, for a valley phonon, if its Berry curvature is nonzero, we can also expect to

observe a valley phonon Hall effect in the presence of an in-plane gradient strain field. Such a valley phonon Hall effect can provide us with another way to observe valley phonons.

With the breaking of spatial inversion symmetry, we observe nonzero phonon Berry curvature at valleys, as shown in Fig. 3(a) (see the Supplemental Material, Sec. VI for the derivation [15]). Bands 2 and 3 have large Berry curvatures at the valleys, while those of bands 1 and 4 are small. Because of the nonzero phonon Berry curvature, applying a strain gradient  $\mathbf{E}_{\text{strain}}$  along the  $x$  direction, phonons excited at a different valley will go to a different transverse direction since  $\mathbf{v}_{\text{anom}} \propto -\mathbf{E}_{\text{strain}} \times \boldsymbol{\Omega}$ , analogous to the electrons. If the photon polarization is reversed, the transverse phonon current would be reversed, as shown in Figs. 3(b) and 3(c). With the accumulation of phonons on one edge, one can measure a temperature difference along

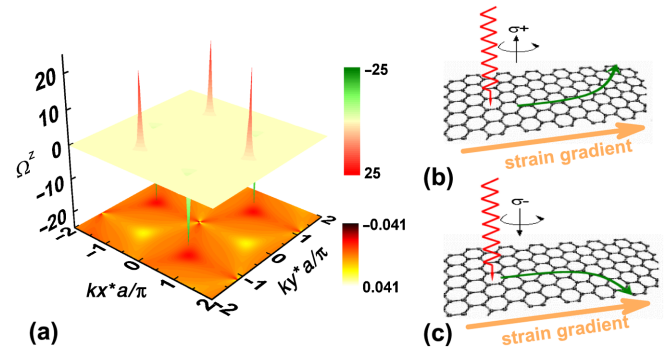


FIG. 3 (color online). Phonon Berry curvature and valley phonon Hall effect in a honeycomb lattice. (a) Berry curvature of band 1 (bottom contour plot) and band 2 (top 3D plot). Band 3 (band 4) has a phonon angular momentum the opposite of that in band 2 (band 1). (b) [(c)] Schematic of the valley phonon Hall effect (the Hall current denoted by the olive curve arrows) under a strain gradient (the orange arrows), where valley phonons are excited by a ray of right-handed or left-handed polarized light (the red wave lines). The parameters are the same as those in Fig. 1.

the transverse direction. The temperature difference changes sign if the circular polarization of the stimulated photon is reversed. The phonon Hall effect has been observed in a paramagnetic insulator [29], where a magnetic field can distort phonon transport; thus, a transverse temperature difference can be observed, which has attracted many studies in this field [30–32]. The Berry curvature induced transverse valley phonon Hall effect at nonmagnetic systems with inversion symmetry broken would attract new applications.

We thank Ji Feng and Gang Zhang for the helpful discussions. We acknowledge support from DOE-DMSE (Grant No. DE-FG03-02ER45958), NBRPC (Grant No. 2012CB-921300), NSFC (Grants No. 91121004 and No. 11574154), and the Welch Foundation (Grant No. F-1255).

- 
- [1] D. Xiao, W. Yao, and Q. Niu, *Phys. Rev. Lett.* **99**, 236809 (2007).
- [2] W. Yao, D. Xiao, and Q. Niu, *Phys. Rev. B* **77**, 235406 (2008).
- [3] D. Xiao, G.-B. Liu, W. Feng, X. Xu, and W. Yao, *Phys. Rev. Lett.* **108**, 196802 (2012).
- [4] T. Cao *et al.*, *Nat. Commun.* **3**, 887 (2012).
- [5] Q. H. Wang, K. Kalantar-Zadeh, A. Kis, J. N. Coleman, and M. S. Strano, *Nat. Nanotechnol.* **7**, 699 (2012).
- [6] K. F. Mak, K. He, J. Shan, and T. F. Heinz, *Nat. Nanotechnol.* **7**, 494 (2012).
- [7] H. Zeng, J. Dai, W. Yao, D. Xiao, and X. Cui, *Nat. Nanotechnol.* **7**, 490 (2012).
- [8] S. Wu *et al.*, *Nat. Phys.* **9**, 149 (2013).
- [9] A. M. Jones *et al.*, *Nat. Nanotechnol.* **8**, 634 (2013).
- [10] X. Xu, W. Yao, D. Xiao, and T. F. Heinz, *Nat. Phys.* **10**, 343 (2014).
- [11] S.-Y. Chen, C. Zheng, M. S. Fuhrer, and J. Yan, *Nano Lett.* **15**, 2526 (2015).
- [12] S. Chen, Q. Wu, C. Mishra, J. Kang, H. Zhang, K. Cho, W. Cai, A. A. Balandin, and R. S. Ruoff, *Nat. Mater.* **11**, 203 (2012).
- [13] S. Y. Zhou, G.-H. Gweon, A. V. Fedorov, P. N. First, W. A. de Heer, D.-H. Lee, F. Guinea, A. H. Castro Neto, and A. Lanzara, *Nat. Mater.* **6**, 770 (2007).
- [14] G. Kim, A.-R. Jang, H. Y. Jeong, Z. Lee, D. J. Kang, and H. S. Shin, *Nano Lett.* **13**, 1834 (2013).
- [15] See Supplemental Material at <http://link.aps.org/supplemental/10.1103/PhysRevLett.115.115502>, which includes Refs. [16–18], for derivations on general phonon polarization and phonon Berry curvature, detailed calculations on graphene and MoS<sub>2</sub>, and discussion of circularly polarized infrared absorption and emission.
- [16] R. Saito, G. Dresselhaus, and M. S. Dresselhaus, *Physical Properties of Carbon Nanotubes* (Imperial College Press, London, 1998).
- [17] J. Callaway, *Quantum Theory of the Solid State*, 2nd ed. (Academic Press, San Diego, 1991).
- [18] G. Giovannetti, P. A. Khomyakov, G. Brocks, P. J. Kelly, and J. van den Brink, *Phys. Rev. B* **76**, 073103 (2007).
- [19] L. Zhang and Q. Niu, *Phys. Rev. Lett.* **112**, 085503 (2014).
- [20] R. Saito, A. Jorio, A. G. Souza Filho, G. Dresselhaus, M. S. Dresselhaus, and M. A. Pimenta, *Phys. Rev. Lett.* **88**, 027401 (2001).
- [21] L. M. Malarda, M. A. Pimenta, G. Dresselhaus, and M. S. Dresselhaus, *Phys. Rep.* **473**, 51 (2009).
- [22] Z. M. Wang, *MoS<sub>2</sub>: Materials, Physics, and Devices* (Springer, Cham, Switzerland, 2014).
- [23] P. Giannozzi *et al.*, *J. Phys. Condens. Matter* **21**, 395502 (2009).
- [24] F. Wu, F. Qu, and A. H. MacDonald, *Phys. Rev. B* **91**, 075310 (2015).
- [25] M.-C. Chang and Q. Niu, *Phys. Rev. B* **53**, 7010 (1996).
- [26] D. Xiao, M.-C. Chang, and Q. Niu, *Rev. Mod. Phys.* **82**, 1959 (2010).
- [27] K. F. Mak, K. L. McGill, J. Park, and P. L. McEuen, *Science* **344**, 1489 (2014).
- [28] R. V. Gorbachev *et al.*, *Science* **346**, 448 (2014).
- [29] C. Strohm, G. L. J. A. Rikken, and P. Wyder, *Phys. Rev. Lett.* **95**, 155901 (2005); A. V. Inyushkin and A. N. Taldenkov, *JETP Lett.* **86**, 379 (2007).
- [30] L. Sheng, D. N. Sheng, and C. S. Ting, *Phys. Rev. Lett.* **96**, 155901 (2006); Y. Kagan and L. A. Maksimov, *Phys. Rev. Lett.* **100**, 145902 (2008).
- [31] J.-S. Wang and L. Zhang, *Phys. Rev. B* **80**, 012301 (2009); L. Zhang, J.-S. Wang, and B. Li, *New J. Phys.* **11**, 113038 (2009); L. Zhang, J. Ren, J.-S. Wang, and B. Li, *Phys. Rev. Lett.* **105**, 225901 (2010); B. K. Agarwalla, L. Zhang, J.-S. Wang, and B. Li, *Eur. Phys. J. B* **81**, 197 (2011); L. Zhang, J. Ren, J.-S. Wang, and B. Li, *J. Phys. Condens. Matter* **23**, 305402 (2011).
- [32] T. Qin, J. Zhou, and J. Shi, *Phys. Rev. B* **86**, 104305 (2012); M. Mori, A. Spencer-Smith, O. P. Sushkov, and S. Maekawa, *Phys. Rev. Lett.* **113**, 265901 (2014).